

CyC3D: Fine-grained Controllable 3D Generation via Cycle Consistency Regularization

Hongbin Xu^{1,2} Chaohui Yu² Feng Xiao¹ Jiazheng Xing² Hai Ci⁴ Weitao Chen² Ming Li^{3*}

¹South China University of Technology

²Alibaba Group

³Guangdong Laboratory of Artificial Intelligence and Digital Economy (SZ)

⁴National University of Technology

*Corresponding Author

Abstract

Despite the remarkable progress of 3D generation, achieving controllability, i.e., ensuring consistency between generated 3D content and input conditions like edge and depth, remains a significant challenge. Existing methods often struggle to maintain accurate alignment, leading to noticeable discrepancies. To address this issue, we propose CyC3D, a new framework that enhances controllable 3D generation by explicitly encouraging cyclic consistency between the second-order 3D content, generated based on extracted signals from the first-order generation, and its original input controls. Specifically, we employ an efficient feed-forward backbone that can generate a 3D object from an input condition and a text prompt. Given an initial viewpoint and a control signal, a novel view is rendered from the generated 3D content, from which the extracted condition is used to regenerate the 3D content. This re-generated output is then rendered back to the initial viewpoint, followed by another round of control signal extraction, forming a cyclic process with two consistency constraints. View consistency ensures coherence between the two generated 3D objects, measured by semantic similarity to accommodate generative diversity. Condition consistency aligns the final extracted signal with the original input control, preserving structural or geometric details throughout the process. Extensive experiments on popular benchmarks demonstrate that CyC3D significantly improves controllability, especially for fine-grained details, outperforming existing methods across various conditions (e.g., +14.17% PSNR for edge, +6.26% PSNR for sketch).

1. Introduction

The creation of 3D models from text descriptions (text-to-3D) or image collections (image-to-3D) is a funda-

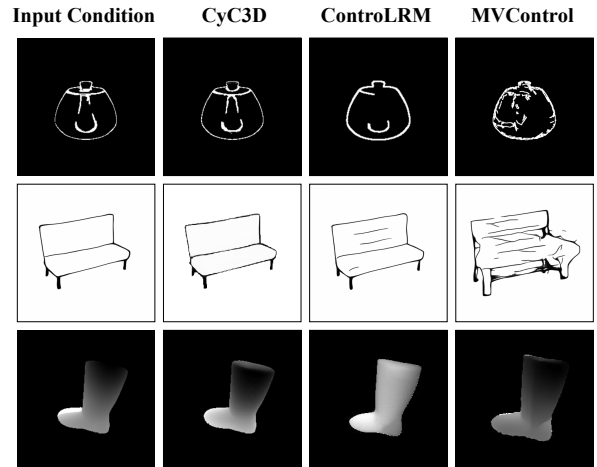


Figure 1. Visualization of input and reconstructed conditions. We feed the input condition to the generation model first and use the generated 3D contents to render the image at the input viewpoint to extract the reconstructed conditions. The difference between the input and the reconstructed conditions can reveal whether the fine-grained controls are reserved in the results.

mental task in computer graphics, attracting growing interest from a wide range of domains, including VR/AR [2], digital game design [32], and filmmaking [30]. The mainstream approaches can be broadly categorized into two groups: optimization-based methods and feed-forward methods. Optimization-based 3D generation methods leverage Score Distillation Sampling (SDS) [20] to iteratively refine 3D objects based on textual or visual inputs, effectively distilling the rich prior knowledge embedded in large pre-trained diffusion models [24]. In contrast, feed-forward 3D generation approaches [5, 11, 12, 19, 28, 29, 36] generate 3D content in a single inference pass, significantly improving efficiency and making real-time applications more feasible.

While significant progress has been made in 3D gener-

2. Related Work

Text-/Image-to-3D Generation. 3D generation can be broadly categorized into optimization-based and feed-forward approaches: (1) Optimization-based methods offer a viable alternative to traditional techniques by circumventing the need for extensive text-to-3D datasets. DreamFusion [20] exemplifies this approach by utilizing SDS loss to optimize neural fields with diffusion priors, resulting in high-quality 3D assets. Despite their effectiveness, these methods often encounter the Janus problem, which arises from inconsistencies between 2D supervision and 3D geometry. (2) Feed-forward models have emerged as a prominent approach for efficient 3D generation, leveraging extensive 3D datasets. Techniques such as LRM [12] and TripoSR [29] utilize transformer architectures to predict NeRF from single-view images, demonstrating high generalization capabilities. Multi-view methods extend these approaches by synthesizing higher-quality 3D models from single-view images using multi-view diffusion models, as demonstrated by SyncDreamer [16] and MVDream [25].

Controllable 3D Generation. Achieving controllability in 3D generation remains a critical objective in the field. Techniques developed for controllable 2D generation have provided valuable insights and methods that are applicable to the more complex domain of controllable 3D generation. Inspired by ControlNet [35], MVControl [15] integrates a trainable control network with a multi-view diffusion model to facilitate controllable multi-view image generation. This method combines coarse Gaussian generation with SDS-based refinement but faces challenges related to model generalization and procedural complexity. ControlLRM [31] addresses these limitations with its end-to-end feed-forward model, ensuring rapid inference and enhanced control precision, thus offering an efficient and effective solution for controllable 3D generation. Building on the advances of ControlNet++ [14] and ControlLRM [35], we improve conditional controls to achieve more sophisticated and nuanced control over the generated 3D assets.

3. CyC3D

As shown in Fig. 3, we present the overall framework of our proposed CyC3D. In Sec. 3.1, we first introduce the feed-forward backbone network for controllable 3D generation in our CyC3D. Then we introduce the condition extractor (Fig. 3(b)) for different conditional controls (e.g. edge, sketch, depth, normal) in Sec. 3.2. In Sec. 3.3, we introduce the design of condition cycle consistency regularization (Fig. 3(c)) to enhance the fined-grained controls. In Sec. 3.4, we further introduce the proposed view cycle consistency regularization (Fig. 3(d)) to stabilize the training and avoid overfitting on the input condition. Finally, we introduce the overall loss in Sec. 3.5.

3.1. Generation Backbone

For controllable 3D generation, our CyC3D can be combined with arbitrary feed-forward backbones (e.g. ControlLRM [31], MVControl [15]). In default, we select ControlLRM [31] as our backbone model. ControlLRM contains a 2D condition extractor and a 3D triplane decoder. (1) The conditional generator in ControlLRM is designed to take both text and 2D visual conditions as inputs. This generator can utilize either a transformer or diffusion backbone to create initial 2D latent representations, which are subsequently transformed into 3D models. (2) The 3D triplane decoder is inherited from a pre-trained large reconstruction model [12]. The triplane transformer decoder employs a unique representation of 3D data by decomposing it into three orthogonal planes (X, Y, and Z). Each plane is processed using transformer layers, which utilize self-attention mechanisms to capture spatial relationships and dependencies within the data.

3.2. Condition Extractor

To ensure the gradient back-propagation of cycle consistency in our CyC3D framework during training, the utilized condition extractor in Fig. 2 should be differentiable. The design of the condition extractor for each condition control is shown as follows:

Canny Condition. As shown in the figure, we extract edge maps using the Canny algorithm [4]. Following [14], a differentiable Canny extractor can be implemented based on Kornia [23] to extract edge maps.

Sketch Condition. Following ControlNet [35], we utilize a pre-trained CNN network to extract sketch conditions from images. Since the CNN network is differentiable, the gradients can be passed backward through the network and back-propagated to the remaining modules.

Depth Condition. In analogy with the sketch condition, we also utilize a pre-trained foundation model (Depth Anything [33]) to extract the depth condition from rendered images. The whole process is differentiable in the cycle consistency pipeline.

Normal Condition. In practice, we find that the existing normal estimation models [1] utilized in ControlNet [35] tends to predict over-smoothed normal maps. It may result in a large gap between the exact 3D shape of the rendered multi-view images and the estimated normal maps. Consequently, we adopt an alternative solution to predict the depth map first and then convert the depth map to normal map via a differentiable module [13]. The great zero-shot generalization ability of large depth-estimation models like Depth-Anything [33] can effectively capture the 3D prior from the image and thus generate accurate normal map.

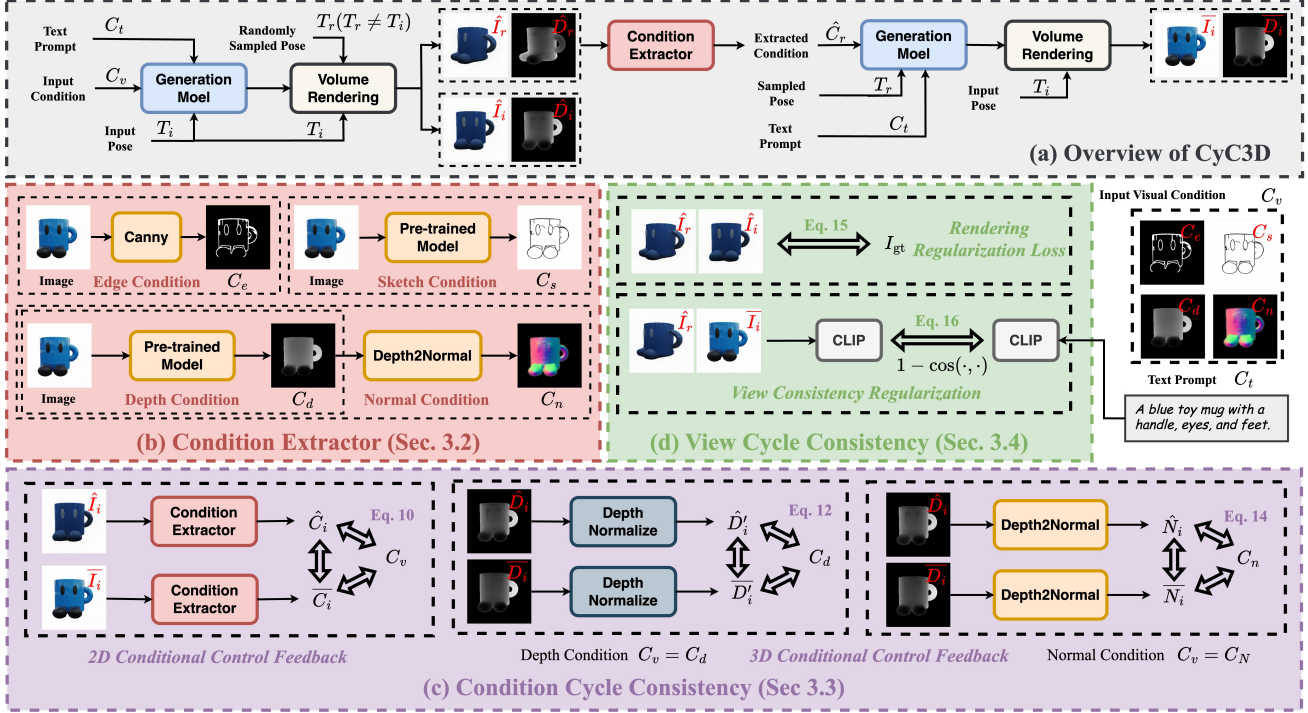


Figure 3. Overall framework of our proposed **CyC3D**. (a) summarize the procedure of our **CyC3D**. (b) shows the condition extractor utilized for different conditional controls (Sec. 3.2). (c) illustrates the condition cycle consistency regularization (Sec. 3.3). (d) introduces the proposed view cycle consistency regularization (Sec. 3.4).

3.3. Condition Cycle Consistency Regularization

Denote the input edge condition as $C_e \in \mathbb{R}^{H \times W}$, the sketch condition as $C_s \in \mathbb{R}^{H \times W}$, the depth condition as $C_d \in \mathbb{R}^{H \times W}$, and the normal condition as $C_n \in \mathbb{R}^{H \times W \times 3}$. The input visual condition is noted as $C_v \in \{C_e, C_s, C_d, C_n\}$. Given the text prompt C_t and the input visual condition as C_v , the generation model outputs the triplane representation $P \in \mathbb{R}^{3 \times C_p \times H_p \times W_p}$ corresponding to the input conditions.

$$P_i = f_{\text{gen}}(C_v, C_t, T_i), \quad (1)$$

where T_i is the camera pose of the input condition, which is usually assumed to be an identity matrix after normalizing all the camera extrinsics to a frontal view. f_{gen} is the backbone generation model for controllable 3D generation.

Given a 3D point $x \in \mathbb{R}^3$, the color and density filed (c, σ) can be obtained via sampling the corresponding features on the triplane P_i : $(c, \sigma) = f_{\text{mlp}}(P_i, x)$. By sampling the points along the viewpoint $T_r \in \mathbb{R}^{4 \times 4}$, we can render the image on view T_r via volume rendering [17]:

$$\hat{I}_r, \hat{D}_r = f_{\text{render}}(P_i, T_r), \quad (2)$$

where T_r is the randomly sampled viewpoints as shown in Fig. 3. \hat{I}_r is the rendered image on view T_r , and \hat{D}_r is the rendered depth map. Then we can use the corresponding condition extractor f_{cond} introduced in Sec. 3.2 and Fig. 3 (b) to extract the condition map on the sampled view T_r :

$$\hat{C}_r = f_{\text{cond}}(\hat{I}_r), \quad (3)$$

where \hat{C}_r is the extracted condition map. Note that the condition extractor f_{cond} is differentiable.

In a second time, we can feed the obtained condition map \hat{C}_r on novel view T_r back to the generation model f_{gen} again:

$$P_r = f_{\text{gen}}(\hat{C}_r, C_t, T_r), \quad (4)$$

where the predicted triplane P_r can further be used to render on the input reference view T_i :

$$\bar{I}_i, \bar{D}_i = f_{\text{render}}(P_r, T_i), \quad (5)$$

where \bar{I}_i is the rendered image on the input reference view, and \bar{D}_i is the rendered depth map. Then we can extract the condition map from the rendered image \bar{I}_i :

$$\bar{C}_i = f_{\text{cond}}(\bar{I}_i), \quad (6)$$

where \bar{C}_i is the generated condition map back on the input reference view.

As shown in Fig. 2 and 3, we can calculate the difference between the reconstructed condition and the input condition to regularize the fine-grained controls. Depending on the type of conditional controls, we also propose two different kinds of conditional cycle-consistency feedbacks as follows:

2D Conditional Control Feedback: If we only consider 2D conditional controls extracted from the rendered images (e.g. Canny map extracted from RGB image), we can use a condition extractor to reconstruct the control signal. The

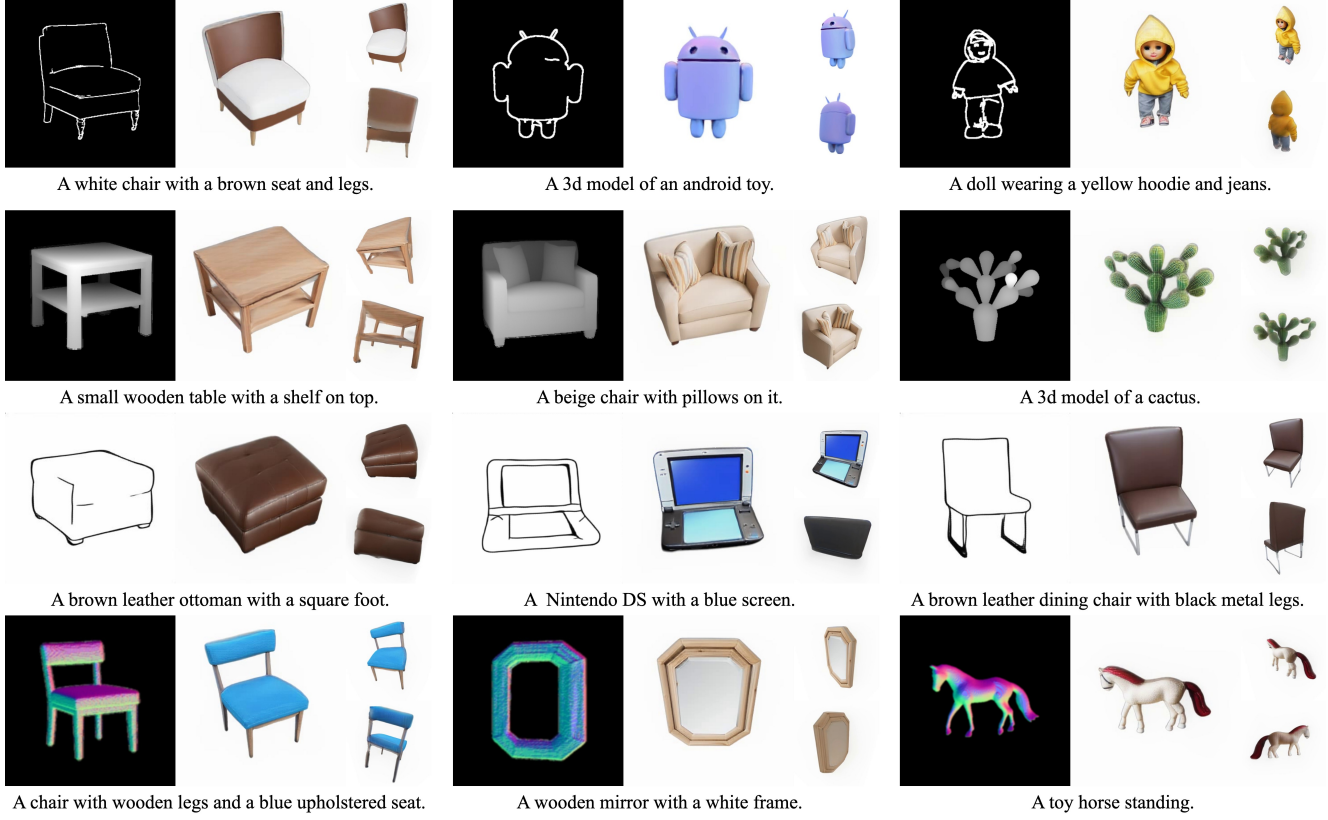


Figure 4. Visualization results of our CyC3D. The input conditions and the rendered images at different views are visualized. Our CyC3D can generate high quality results with consistent conditional controls.

generated condition map \overline{C}_i via Eq. 6 should be consistent with the original condition map C_v on the input reference view.

$$L_{\text{cond}} = \sum_{T_r} \|\overline{C}_i - C_v\|_2^2. \quad (7)$$

If the randomly sampled camera pose T_r equals to the input viewpoint T_i , the two-step inference in cycle consistency will be degraded to a single one (as shown in Fig. 3 (c)), saving the computation cost:

$$\hat{I}_i, \hat{D}_i = f_{\text{render}}(f_{\text{gen}}(C_v, C_t, T_i), T_i), \quad (8)$$

$$\hat{C}_i = f_{\text{cond}}(\hat{I}_i), \quad (9)$$

where \hat{C}_i is the extracted condition map on the input reference view. In this way, we can modify Eq. 7 as:

$$L_{\text{cond}} = \sum_{T_r \neq T_i} \|\overline{C}_i - C_v\|_2^2 + \|\hat{C}_i - C_v\|_2^2. \quad (10)$$

3D Conditional Control Feedback: If we consider 3D conditional controls like depth or normal conditions, the 3D shape of the generated objects should be regularized as well for a fine-grained control.

(1) If the input condition is depth map ($C_v = C_d$), the explicit consistency on the rendered depth map and the in-

put conditional depth map can be calculated as follows:

$$L_{\text{cond-d}} = \sum_{T_r} \|f_{\text{norm}}(\overline{D}_i) - C_d\|_2^2, \quad (11)$$

where f_{norm} is the depth normalizing function. Since the rendered depth \overline{D}_i and the input depth C_d have a gap in the scale of depth, we utilize f_{norm} to normalize them to the same scale and calculate a scale-agnostic loss following [22].

In analogy with Eq. 10, when the randomly sampled camera pose T_r equals to the input viewpoint T_i , there is no need to run the inference twice during propagation. We can modify Eq. 11 as follows:

$$L_{\text{cond-d}} = \sum_{T_r \neq T_i} \|f_{\text{norm}}(\overline{D}_i) - C_d\|_2^2 + \|f_{\text{norm}}(\hat{D}_i) - C_d\|_2^2, \quad (12)$$

where \hat{D}_i can be obtained from Eq. 8.

(2) If the input condition is normal map ($C_v = C_n$), the explicit depth-normal consistency can be further calculated as follows:

$$L_{\text{cond-n}} = \sum_{T_r} \|f_{\text{d2n}}(\overline{D}_i) - C_n\|_2^2, \quad (13)$$

where f_{d2n} is a differentiable module [13] that can convert the depth map to a unified normal map.

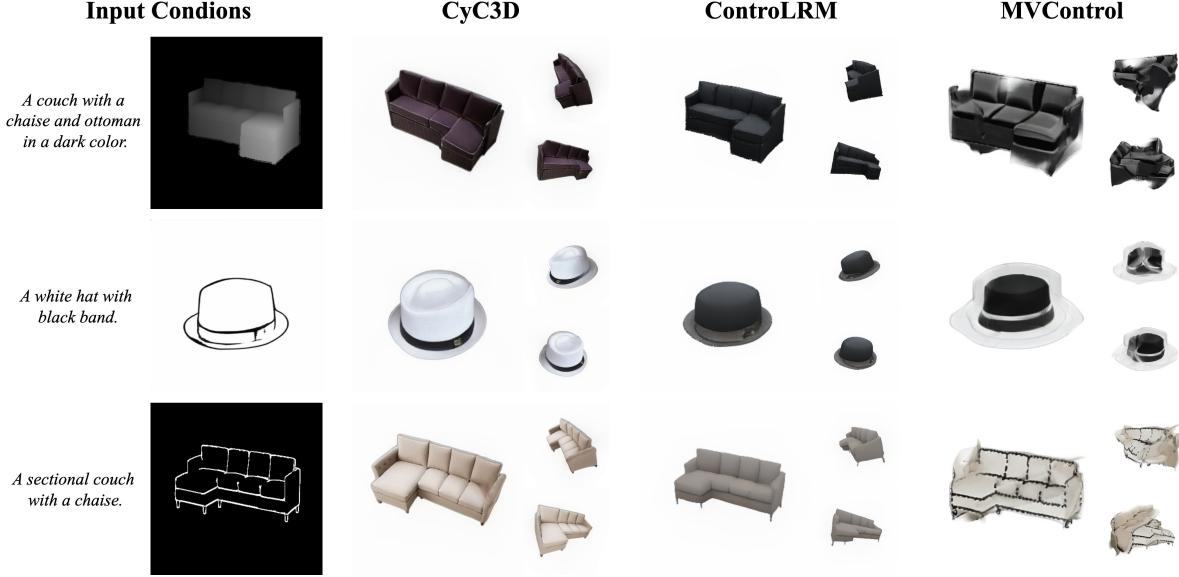


Figure 5. Qualitative comparison among our CyC3D and the other state-of-the-art controllable 3D generation methods.

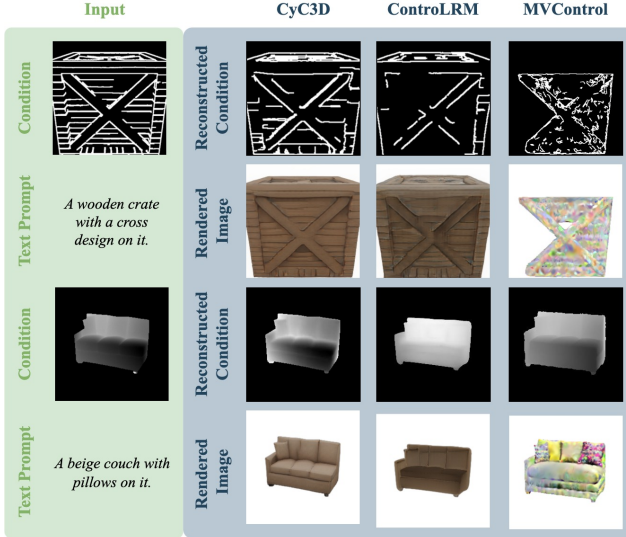


Figure 6. Qualitative comparison of controllability among our CyC3D and the existing state-of-the-art methods in controllable 3D generation.

In analogy with Eq. 10 and 12, when the randomly sampled camera pose T_r equals to the input viewpoint T_i , there is no need to run the inference twice during propagation. We can thus modify Eq. 13 as follows:

$$L_{\text{cond-n}} = \sum_{T_r \neq T_i} \|f_{\text{d2n}}(\bar{D}_i) - C_n\|_2^2 + \|f_{\text{d2n}}(\hat{D}_i) - C_n\|_2^2, \quad (14)$$

where \hat{D}_i can be obtained from Eq. 8.

3.4. View Cycle Consistency Regularization

Since the condition cycle consistency regularization (Sec. 3.3) is a strong constraint that enforces the reconstructed and the input conditions to be as similar as possible, only

using this loss might lead to overfitting towards the input viewpoint. If the generated 3D content from the initial view fails, the remaining processes might be misled to a wrong cross-view mapping. Only using the condition cycle consistency on the input view can not handle this issue, and the semantic multi-view consistency might be ignored during optimization. Consequently, we propose View Cycle Consistency Regularization to ensure convergence.

Rendering Regularization Loss: To regularize the possible failures in generation, the image reconstruction loss between the rendered images from generated 3D contents and the ground truth images on different views are used to supervise the generation model f_{gen} :

$$L_{\text{render}} = \sum_{T_l} \|f_{\text{render}}(f_{\text{gen}}(C_v, C_i, T_i), T_l) - I_l^{\text{gt}}\|_2^2, \quad (15)$$

where T_l means the pre-defined ground truth viewpoints in the multi-view dataset, and I_l^{gt} is the corresponding ground truth image. Note that this constraint can only be used in the first-time feedforward computation of the generation model. Because the randomness of the generation model might be depressed if enforcing the first-time and second-time generated 3D contents to be the same.

Semantic Consistency Loss: We utilize the text prompt C_t to regularize the semantic consistency of different stages.

$$L_{\text{clip}} = \sum_{T_r} (1 - \cos(f_{\text{clip-t}}(C_t), f_{\text{clip-i}}(\hat{I}_r))) + (1 - \cos(f_{\text{clip-t}}(C_t), f_{\text{clip-i}}(\bar{I}_i))). \quad (16)$$

View Consistency Regularization: The overall view cycle consistency loss can be computed as follows:

$$L_{\text{view}} = L_{\text{render}} + \alpha \cdot L_{\text{clip}}, \quad (17)$$

where α is the set to 5.0 following [31] to balance the scale of different terms as default.

3.5. Overall Loss

Finally, the overall loss is the combination of the aforementioned losses:

$$L_{\text{total}} = \begin{cases} L_{\text{view}} + \lambda \cdot L_{\text{cond}} + \beta \cdot L_{\text{cond-d}}, & \text{if } C_v = C_d \\ L_{\text{view}} + \lambda \cdot L_{\text{cond}} + \beta \cdot L_{\text{cond-n}}, & \text{if } C_v = C_n \\ L_{\text{view}} + \lambda \cdot L_{\text{cond}}, & \text{otherwise} \end{cases} \quad (18)$$

where λ is set to 1.0 in default, and β is set to 0.1 for regularization.

4. Experiment

4.1. Implementation Details

Datasets. Our training dataset is the training split of G-Objaverse (**GOBJ**) dataset [21], a sub-set of Objaverse [8]. Following the selection principle of [15], we utilize the test samples collected by [31] gathered from 2 different datasets for zero-shot evaluation: 80 samples from Google Scanned Objects dataset (**GSO**) [9], and 80 samples from Amazon Berkeley Objects dataset (**ABO**) [7].

Training Details. In analogy with [31], we initialize our network with the weights from pretrained OpenLRM-base [12]. For CyC3D-T, the conditional backbone is a transformer-based network; For CyC3D-D, the conditional backbone is a diffusion-based network. The training might cost 2 days for CyC3D-T and 3 days for CyC3D-D on 32 Nvidia V100-32G GPUs. More details are provided in the appendix.

Evaluation and Metrics. For the task of controllable 3D generation task, we consider 4 different conditions: edge, sketch, depth, and normal. For each condition, we evaluate the controllability by measuring the similarity between the input conditions and the extracted conditions from generated 3D contents following [31]. For edge/sketch condition, we utilize **PSNR**, **SSIM**, and **MSE** as evaluation metrics; For depth/normal condition, we utilize **MSE** to measure the similarity. In analogy with [14], the large foundation models in monocular depth estimation are used to capture the depth priors for model-based evaluation. If Midas [22] is used, the metric is noted as **M-MSE**. If ZoeDepth [3] is used, the metric is noted as **Z-MSE**. Following [31], the depth consistency in 3D space compares the difference between rendered depth map and the input condition depth map, noted as **R-MSE**. In analogy with [14], the metric of **NB-MSE** uses the pre-trained model (Normal-BAE [1]) in surface normal estimation to assess the normal consistency. Furthermore, we also evaluate the depth-normal consistency between the rendered depth map and the input normal maps following [31], noted as **DN-CON**. Please refer

to more detailed introduction of these evaluation metrics in the appendix.

4.2. Experimental Results

Qualitative Results. We provide qualitative results of our CyC3D in Fig. 4. The backbone is inherited from ControlRM [31], and the diffusion model is replaced with a pre-trained ControlNet. As the figure shows, our method not only performs well in generating high quality 3D contents but also in preserving details in conditional controls. Furthermore, we also compare the qualitative results of our CyC3D with other state-of-the-art methods including ControlRM [31] and MVControl [15] in Fig. 5.

Controllability Evaluation. The comparisons of controllability with state-of-the-art controllable 3D generation methods on **GSO/ABO** benchmarks are presented in Tab. 1/2. Following [31], we report the controllability metrics discussed in Sec. 4.1 on all conditional controls. From the tables, we can find that our CyC3D can achieve state-of-the-art performance in the quantitative comparison with other baselines. For example, the R-MSE of our CyC3D-D is 0.0060, which is much lower than the baselines of ControlRM-D (0.0650 R-MSE). Furthermore, we also provide qualitative comparison of controllability in Fig. 6.

Generation Evaluation. To investigate whether improving controllability compromises generation quality, we provide the quantitative results of Fréchet Inception Distance (FID) [10] and CLIP-score [18] following [15] in Tab. 3. We report CLIP-I metric to quantify image similarity between reference and rendered images, and CLIP-T metric to evaluate text-image alignment using textual annotations. In rigorous zero-shot generalization experiments of cross-domain transitions towards GSO and ABO, our proposed CyC3D demonstrates statistically significant improvements over existing methods. Furthermore, from the qualitative results in Fig. 5, our CyC3D can generate better results with higher quality and consistency than existing methods.

Comparison with ControlNet-based Baselines. For a fair comparison, we also provide experimental results compared with ControlNet combined with image-to-3D reconstruction models. The images produced by ControlNet are processed through image-to-3D reconstruction models to synthesize 3D assets, with foreground segmentation implemented using Rembg for background removal. The quantitative evaluation results on the GSO benchmark are presented in Tab. 4, incorporating state-of-the-art image-to-3D systems including OpenLRM [12], TGS [36], and TripoSR [29] as comparative baselines.

4.3. Ablation Study

Effect of Condition Cycle Consistency. To evaluate the effectiveness of 2D conditional control feedback (e.g. Eq. 10 for edge/sketch), we provide ablation experiments in Tab.

Methods	Edge			Sketch			Depth			Normal	
	PSNR \uparrow	SSIM \uparrow	MSE \downarrow	PSNR \uparrow	SSIM \uparrow	MSE \downarrow	M-MSE \downarrow	Z-MSE \downarrow	R-MSE \downarrow	NB-MSE \downarrow	DN-CON \downarrow
GSGEN [6]	13.01	0.780	0.0526	15.07	0.772	0.0322	0.1277	0.1268	0.0311	0.0230	0.0497
GaussianDreamer [34]	12.41	0.766	0.0597	14.58	0.792	0.0362	0.0740	0.0947	0.0391	0.0225	0.0366
DreamGaussian [26]	9.94	0.686	0.1048	14.42	0.765	0.0380	0.0980	0.0916	0.0406	0.0216	0.0335
VolumeDiffusion [28]	13.25	0.818	0.0497	16.50	0.836	0.0231	0.1202	0.0953	0.0531	0.0190	0.0172
3DTopia [11]	9.63	0.704	0.1134	15.54	0.801	0.0287	0.1193	0.1064	0.0420	0.0268	0.0372
MVControl [15]	10.44	0.723	0.0952	14.51	0.746	0.0370	0.0555	0.0645	0.0160	0.0209	0.0315
ControlLRM-T [31]	12.43	0.836	0.0607	17.17	0.836	0.0202	0.0567	0.0713	0.0599	0.0120	0.0359
ControlLRM-D [31]	12.47	0.837	0.0600	17.23	0.837	0.0197	0.0383	0.0546	0.0650	0.0119	0.0357
CyC3D-T (Ours)	15.17	0.885	0.0342	18.31	0.889	0.0159	0.0051	0.0037	0.0065	0.0027	0.0062
CyC3D-D (Ours)	15.09	0.885	0.0347	18.38	0.890	0.0156	0.0051	0.0041	0.0060	0.0028	0.0060

Table 1. Quantitative comparison of controllability with state-of-the-art controllable 3D generation methods on **GSO** benchmark. \uparrow denotes higher result is better, while \downarrow means lower is better. The best results are highlighted in **bold**. We provide the results of four different conditions: edge, sketch, depth, and normal. Our CyC3D-T/D achieves significant controllability improvements in the table.

Methods	Edge			Sketch			Depth			Normal	
	PSNR \uparrow	SSIM \uparrow	MSE \downarrow	PSNR \uparrow	SSIM \uparrow	MSE \downarrow	M-MSE \downarrow	Z-MSE \downarrow	R-MSE \downarrow	NB-MSE \downarrow	DN-CON \downarrow
GSGEN [6]	12.75	0.737	0.0614	14.25	0.744	0.0384	0.1004	0.0967	0.0463	0.0171	0.0479
GaussianDreamer [34]	11.92	0.736	0.0699	13.75	0.734	0.0439	0.0809	0.1061	0.0521	0.0188	0.0463
DreamGaussian [26]	9.38	0.683	0.1178	12.90	0.716	0.0523	0.1267	0.0762	0.0433	0.0188	0.0349
VolumeDiffusion [28]	12.58	0.734	0.0619	15.03	0.780	0.0321	0.1007	0.1198	0.0671	0.0188	0.0264
3DTopia [11]	8.48	0.633	0.1469	14.41	0.741	0.0372	0.1916	0.1844	0.0559	0.0346	0.0418
MVControl [15]	9.52	0.656	0.1161	13.34	0.686	0.0479	0.0454	0.0467	0.0181	0.0133	0.0350
ControlLRM-T [31]	10.49	0.552	0.0909	15.77	0.777	0.0272	0.0514	0.0497	0.0700	0.0136	0.0572
ControlLRM-D [31]	11.51	0.592	0.0725	15.80	0.778	0.0269	0.0493	0.0545	0.0661	0.0158	0.0548
CyC3D-T (Ours)	12.98	0.756	0.0540	16.55	0.847	0.0225	0.0080	0.0078	0.0102	0.0029	0.0102
CyC3D-D (Ours)	12.99	0.755	0.0539	16.45	0.845	0.0231	0.0075	0.0087	0.0091	0.0030	0.0109

Table 2. Quantitative comparison of controllability with state-of-the-art controllable 3D generation methods on **ABO** benchmark. \uparrow denotes higher result is better, while \downarrow means lower is better. The best results are highlighted in **bold**. We provide the results of four different conditions: edge, sketch, depth, and normal. Our CyC3D-T/D achieves significant controllability improvements in the table.

Methods	GOBJ \rightarrow GSO			GOBJ \rightarrow ABO		
	FID \downarrow	CLIP-I \uparrow	CLIP-T \uparrow	FID \downarrow	CLIP-I \uparrow	CLIP-T \uparrow
GSGEN [6]	344.61	0.740	0.289	366.47	0.669	0.259
GaussianDreamer [34]	278.70	0.810	0.300	225.38	0.787	0.277
DreamGaussian [26]	359.65	0.760	0.279	392.95	0.723	0.247
VolumeDiffusion [28]	299.61	0.715	0.259	350.46	0.679	0.242
3DTopia [11]	331.39	0.727	0.283	231.55	0.751	0.272
MVControl [15]	278.08	0.816	0.288	217.97	0.802	0.291
ControlLRM-T [31]	260.75	0.846	0.289	202.14	0.827	0.282
ControlLRM-D [31]	171.13	0.838	0.302	181.84	0.836	0.292
CyC3D-T (Ours)	255.30	0.840	0.295	196.55	0.836	0.291
CyC3D-D (Ours)	168.71	0.846	0.303	183.84	0.842	0.293

Table 3. Generation quality (FID) and CLIP score (CLIP-I, CLIP-T) comparison with state-of-the-art controllable 3D generation methods **GSO**, and **ABO** benchmarks. \uparrow means higher result is better, while \downarrow means lower is better. The best results are emphasized in **bold**. We provide the average results of 4 different conditions (edge, sketch, depth, and normal) in the table.

Methods	Control				Quality		
	Edge \downarrow	Sketch \downarrow	Depth \downarrow	Normal \downarrow	FID \downarrow	CLIP-I \uparrow	CLIP-T \uparrow
ControlNet+OpenLRM-S [12]	0.1069	0.0459	0.1333	0.0255	268.7	0.807	0.292
ControlNet+OpenLRM-B [12]	0.0897	0.0452	0.1312	0.0206	258.04	0.822	0.293
ControlNet+OpenLRM-L [12]	0.0792	0.0447	0.1383	0.0226	256.43	0.824	0.294
ControlNet+TGS [36]	0.0523	0.0417	0.1403	0.0208	258.86	0.841	0.295
ControlNet+TripoSR [29]	0.0978	0.0421	0.1188	0.0241	261.76	0.835	0.289
MVControlNet+LGM [15]	0.0952	0.0370	0.0160	0.0315	278.08	0.816	0.288
CyC3D-T (Ours)	0.0342	0.0159	0.0065	0.0062	255.30	0.840	0.295
CyC3D-D (Ours)	0.0347	0.0156	0.0060	0.0060	168.71	0.846	0.303

Table 4. Comparison with ControlNet-based baselines (ControlNet + Image-to-3D methods) on **GSO** benchmark.

5. Furthermore, we also provide ablation results of 3D conditional control feedback (Eq. 12 for depth, Eq. 14 for normal) in Tab. 6. As the tables show, each term of condition cycle consistency can effectively improve the controllability upon different conditional controls.

Loss	Edge			Sketch		
	PSNR	SSIM	MSE	PSNR	SSIM	MSE
w/o L_{cond}	12.87	0.841	0.0570	17.52	0.888	0.0187
w L_{cond}	15.09	0.885	0.0347	18.38	0.890	0.0156

Table 5. Ablation experiments of 2D condition cycle consistency.

Loss	Depth			Loss	Normal	
	M-MSE	Z-MSE	R-MSE		NB-MSE	DN-CON
w/o L_{cond}	0.0383	0.0546	0.0650	w/o L_{cond}	0.0034	0.0205
w L_{cond}	0.0192	0.0241	0.0321	w L_{cond}	0.0023	0.0187
w $L_{cond} + L_{cond-d}$	0.0051	0.0041	0.0060	w $L_{cond} + L_{cond-n}$	0.0011	0.0056

Table 6. Ablation experiments of 3D condition cycle consistency.



Figure 7. Ablation experiments of view cycle consistency.

Effect of View Cycle Consistency. To evaluate the effectiveness of view cycle consistency feedback (e.g. Eq. 17), we provide qualitative ablation results in Fig. 7. As the figure shows, without view cycle consistency regularization, the generated 3D contents might be overfitting to the input viewpoint. Though the rendered results in the input view is reasonable, the lack of regularization on the remaining views might lead to a low-quality 3D shape.

5. Conclusion

In this paper, we propose CyC3D, a novel framework for improving the controllability during 3D generation guided by different conditional controls (edge/sketch/depth/normal). The core idea is the cycle-view consistency which ensures accurate alignment between input conditions and generated models by rendering the generated 3D content from various viewpoints and re-extracting the conditions from these rendered views to feed back into the generation process. The quantitative and qualitative evaluation results on GSO and ABO benchmarks show the state-of-the-art controllability of CyC3D.

References

- [1] Gwangbin Bae, Ignas Budvytis, and Roberto Cipolla. Estimating and exploiting the aleatoric uncertainty in surface normal estimation. In *Proceedings of the IEEE/CVF International Conference on Computer Vision*, pages 13137–13146, 2021. 3, 7
- [2] Majid Behravan. Generative ai framework for 3d object generation in augmented reality. *arXiv preprint arXiv:2502.15869*, 2025. 1
- [3] Shariq Farooq Bhat, Reiner Birkel, Diana Wofk, Peter Wonka, and Matthias Müller. Zoedepth: Zero-shot transfer by combining relative and metric depth. *arXiv preprint arXiv:2302.12288*, 2023. 7
- [4] John Canny. A computational approach to edge detection. *IEEE Transactions on pattern analysis and machine intelligence*, (6):679–698, 1986. 3
- [5] Anpei Chen, Haofei Xu, Stefano Esposito, Siyu Tang, and Andreas Geiger. Lara: Efficient large-baseline radiance fields. In *European Conference on Computer Vision*, pages 338–355. Springer, 2025. 1
- [6] Zilong Chen, Feng Wang, Yikai Wang, and Huaping Liu. Text-to-3d using gaussian splatting. In *Proceedings of the IEEE/CVF Conference on Computer Vision and Pattern Recognition*, pages 21401–21412, 2024. 8
- [7] Jasmine Collins, Shubham Goel, Kenan Deng, Achleshwar Luthra, Leon Xu, Erhan Gundogdu, Xi Zhang, Tomas F Yago Vicente, Thomas Dideriksen, Himanshu Arora, et al. Abo: Dataset and benchmarks for real-world 3d object understanding. In *Proceedings of the IEEE/CVF conference on computer vision and pattern recognition*, pages 21126–21136, 2022. 7
- [8] Matt Deitke, Dustin Schwenk, Jordi Salvador, Luca Weihs, Oscar Michel, Eli VanderBilt, Ludwig Schmidt, Kiana Ehsani, Aniruddha Kembhavi, and Ali Farhadi. Objaverse: A universe of annotated 3d objects. In *Proceedings of the IEEE/CVF Conference on Computer Vision and Pattern Recognition*, pages 13142–13153, 2023. 7
- [9] Laura Downs, Anthony Francis, Nate Koenig, Brandon Kinman, Ryan Hickman, Krista Reymann, Thomas B McHugh, and Vincent Vanhoucke. Google scanned objects: A high-quality dataset of 3d scanned household items. In *2022 International Conference on Robotics and Automation (ICRA)*, pages 2553–2560. IEEE, 2022. 7
- [10] Martin Heusel, Hubert Ramsauer, Thomas Unterthiner, Bernhard Nessler, and Sepp Hochreiter. Gans trained by a two time-scale update rule converge to a local nash equilibrium. *Advances in neural information processing systems*, 30, 2017. 7
- [11] Fangzhou Hong, Jiaxiang Tang, Ziang Cao, Min Shi, Tong Wu, Zhaoxi Chen, Shuai Yang, Tengfei Wang, Liang Pan, Dahua Lin, et al. 3dtopia: Large text-to-3d generation model with hybrid diffusion priors. *arXiv preprint arXiv:2403.02234*, 2024. 1, 8
- [12] Yicong Hong, Kai Zhang, Jiuxiang Gu, Sai Bi, Yang Zhou, Difan Liu, Feng Liu, Kalyan Sunkavalli, Trung Bui, and Hao Tan. Lrm: Large reconstruction model for single image to 3d. *arXiv preprint arXiv:2311.04400*, 2023. 1, 3, 7, 8
- [13] Baichuan Huang, Hongwei Yi, Can Huang, Yijia He, Jingbin Liu, and Xiao Liu. M3vsnet: Unsupervised multi-metric multi-view stereo network. In *2021 IEEE International Conference on Image Processing (ICIP)*, pages 3163–3167. IEEE, 2021. 3, 5
- [14] Ming Li, Taojiannan Yang, Huafeng Kuang, Jie Wu, Zhaoning Wang, Xuefeng Xiao, and Chen Chen. Controlnet++: Improving conditional controls with efficient consistency feedback. In *European Conference on Computer Vision*, pages 129–147. Springer, 2025. 3, 7
- [15] Zhiqi Li, Yiming Chen, Lingzhe Zhao, and Peidong Liu. Controllable text-to-3d generation via surface-aligned gaussian splatting. *arXiv preprint arXiv:2403.09981*, 2024. 2, 3, 7, 8
- [16] Yuan Liu, Cheng Lin, Zijiao Zeng, Xiaoxiao Long, Lingjie Liu, Taku Komura, and Wenping Wang. Syncdreamer: Generating multiview-consistent images from a single-view image. *arXiv preprint arXiv:2309.03453*, 2023. 3
- [17] Ben Mildenhall, Pratul P Srinivasan, Matthew Tancik, Jonathan T Barron, Ravi Ramamoorthi, and Ren Ng. Nerf: Representing scenes as neural radiance fields for view synthesis. *Communications of the ACM*, 65(1):99–106, 2021. 4
- [18] Nasir Mohammad Khalid, Tianhao Xie, Eugene Belilovsky, and Tiberiu Popa. Clip-mesh: Generating textured meshes from text using pretrained image-text models. In *SIGGRAPH Asia 2022 conference papers*, pages 1–8, 2022. 7
- [19] Alex Nichol, Heewoo Jun, Pratul Dhariwal, Pamela Mishkin, and Mark Chen. Point-e: A system for generating 3d point clouds from complex prompts. *arXiv preprint arXiv:2212.08751*, 2022. 1
- [20] Ben Poole, Ajay Jain, Jonathan T Barron, and Ben Mildenhall. Dreamfusion: Text-to-3d using 2d diffusion. *arXiv preprint arXiv:2209.14988*, 2022. 1, 3
- [21] Lingteng Qiu, Guanying Chen, Xiaodong Gu, Qi Zuo, Mutian Xu, Yushuang Wu, Weihao Yuan, Zilong Dong, Liefeng Bo, and Xiaoguang Han. Richdreamer: A generalizable normal-depth diffusion model for detail richness in text-to-3d. In *Proceedings of the IEEE/CVF Conference on Computer Vision and Pattern Recognition*, pages 9914–9925, 2024. 7
- [22] René Ranftl, Katrin Lasinger, David Hafner, Konrad Schindler, and Vladlen Koltun. Towards robust monocular

- depth estimation: Mixing datasets for zero-shot cross-dataset transfer. *IEEE transactions on pattern analysis and machine intelligence*, 44(3):1623–1637, 2020. 5, 7
- [23] Edgar Riba, Dmytro Mishkin, Daniel Ponsa, Ethan Rublee, and Gary Bradski. Kornia: an open source differentiable computer vision library for pytorch. In *Proceedings of the IEEE/CVF Winter Conference on Applications of Computer Vision*, pages 3674–3683, 2020. 3
- [24] Robin Rombach, Andreas Blattmann, Dominik Lorenz, Patrick Esser, and Björn Ommer. High-resolution image synthesis with latent diffusion models. In *Proceedings of the IEEE/CVF conference on computer vision and pattern recognition*, pages 10684–10695, 2022. 1
- [25] Yichun Shi, Peng Wang, Jianglong Ye, Mai Long, Kejie Li, and Xiao Yang. Mvdream: Multi-view diffusion for 3d generation. *arXiv preprint arXiv:2308.16512*, 2023. 2, 3
- [26] Jiaxiang Tang, Jiawei Ren, Hang Zhou, Ziwei Liu, and Gang Zeng. Dreamgaussian: Generative gaussian splatting for efficient 3d content creation. *arXiv preprint arXiv:2309.16653*, 2023. 8
- [27] Jiaxiang Tang, Zhaoxi Chen, Xiaokang Chen, Tengfei Wang, Gang Zeng, and Ziwei Liu. Lgm: Large multi-view gaussian model for high-resolution 3d content creation. In *European Conference on Computer Vision*, pages 1–18. Springer, 2025. 2
- [28] Zhicong Tang, Shuyang Gu, Chunyu Wang, Ting Zhang, Jianmin Bao, Dong Chen, and Baining Guo. Volumediffusion: Flexible text-to-3d generation with efficient volumetric encoder. *arXiv preprint arXiv:2312.11459*, 2023. 1, 8
- [29] Dmitry Tochilkin, David Pankratz, Zexiang Liu, Zixuan Huang, Adam Letts, Yangguang Li, Ding Liang, Christian Laforte, Varun Jampani, and Yan-Pei Cao. Triposr: Fast 3d object reconstruction from a single image. *arXiv preprint arXiv:2403.02151*, 2024. 1, 3, 7, 8
- [30] Qinghe Wang, Yawen Luo, Xiaoyu Shi, Xu Jia, Huchuan Lu, Tianfan Xue, Xintao Wang, Pengfei Wan, Di Zhang, and Kun Gai. Cinemaster: A 3d-aware and controllable framework for cinematic text-to-video generation. *arXiv preprint arXiv:2502.08639*, 2025. 1
- [31] Hongbin Xu, Weitao Chen, Zhipeng Zhou, Feng Xiao, Baigui Sun, Mike Zheng Shou, and Wenxiong Kang. Controlrm: Fast and controllable 3d generation via large reconstruction model. *arXiv preprint arXiv:2410.09592*, 2024. 2, 3, 7, 8
- [32] Yongzhi Xu, Yonhon Ng, Yifu Wang, Inkyu Sa, Yunfei Duan, Yang Li, Pan Ji, and Hongdong Li. Sketch2scene: Automatic generation of interactive 3d game scenes from user’s casual sketches. *arXiv preprint arXiv:2408.04567*, 2024. 1
- [33] Lihe Yang, Bingyi Kang, Zilong Huang, Zhen Zhao, Xiaogang Xu, Jiashi Feng, and Hengshuang Zhao. Depth anything v2. *arXiv preprint arXiv:2406.09414*, 2024. 3
- [34] Taoran Yi, Jiemin Fang, Junjie Wang, Guanjun Wu, Lingxi Xie, Xiaopeng Zhang, Wenyu Liu, Qi Tian, and Xinggang Wang. Gaussiandreamer: Fast generation from text to 3d gaussians by bridging 2d and 3d diffusion models. In *Proceedings of the IEEE/CVF Conference on Computer Vision and Pattern Recognition*, pages 6796–6807, 2024. 8
- [35] Lvmin Zhang, Anyi Rao, and Maneesh Agrawala. Adding conditional control to text-to-image diffusion models. In *Proceedings of the IEEE/CVF International Conference on Computer Vision*, pages 3836–3847, 2023. 3
- [36] Zi-Xin Zou, Zhipeng Yu, Yuan-Chen Guo, Yangguang Li, Ding Liang, Yan-Pei Cao, and Song-Hai Zhang. Triplane meets gaussian splatting: Fast and generalizable single-view 3d reconstruction with transformers. In *Proceedings of the IEEE/CVF Conference on Computer Vision and Pattern Recognition*, pages 10324–10335, 2024. 1, 7, 8